Multivariate Analysis and Anomaly Detection of U.S. Reservoir Sedimentation Dataset

Alejandra Botero-Acosta [a,1], Amanda L. Cox, M. ASCE [2], Vasit Sagan [3], Ibrahim Demir [4], Marian Muste [5], Paul Boyd [6], and Chandra Pathak [7]

[a] Corresponding Author

[1] Research Scientist, WATER Institute, Saint Louis Univ., St. Louis, MO 63103. E-mail: alejandra.boteroacosta@slu.edu

[2] Associate Professor, WATER Institute, Saint Louis Univ., St. Louis, MO 63103. E-mail: amanda.cox@slu.edu

[3] Associate Professor, Taylor Geospatial Institute, Saint Louis Univ., St. Louis, MO 63103. E-mail: vasit.sagan@slu.edu

[4] Associate Professor, Civil and Environmental Engineering, Univ. of Iowa, Iowa City, IA 52242. E-mail: ibrahim-demir@uiowa.edu

[5] Research Engineer, IIHR Hydroscience and Engineering, Univ. of Iowa, Iowa City, IA 52242. E-mail: marian-muste@uiowa.edu

[6] Hydraulic Engineer, Omaha District, US Army Corps of Engineers, Omaha, NE 68138. E-mail: Paul.M.Boyd@usace.army.mil

[7] Hydrologic and Hydraulic Engineer, Headquarters, US Army Corps of Engineers, Washington DC 20314. E-mail: Chandra.S.Pathak@usace.army.mil

This manuscript is an EarthArXiv preprint and has been submitted for possible publication in the peer-reviewed ASCE Journal of Hydrologic Engineering. Subsequent versions of this manuscript may have slightly different content. Please feel free to contact the corresponding author for feedback.

Abstract: Sedimentation processes in reservoirs can jeopardize their functionality and compromise dam safety. Climate change and associated hydrologic uncertainty are introducing additional stressors to US reservoirs, and data-driven indicators of climate impacts on erosion and sedimentation processes at reservoirs and associate watersheds are crucial to evaluate reservoir's aggradation and life expectancy. The US Army Corps of Engineers (USACE) developed the Enhancing Reservoir Sedimentation Information for Climate Preparedness and Resilience (RSI) system to consolidate historical information of elevation-capacity surveys. However, the multiple surveying technologies, protocols, and analysis methods used over the service life of reservoirs can impact the data quality of the RSI system. The objective of this study was to develop a methodology to detect anomalous records and identify multivariate relationships between historical sedimentation data for 184 US reservoirs and associated watershed variables. For this, unsupervised machine learning techniques such as Principal Component Analysis (PCA), Autonomous Anomaly Detection (AAD), and Kolmogorov-Smirnov and Efron anomaly detection (KSE) were implemented. PCA results indicated that reservoirs in the Mediterranean California ecoregion although experiencing substantial extreme precipitation events, had small basin areas and curve number (CN) values that reflected in small capacity losses, contrasting with larger capacity losses found at reservoirs in the Great Plains and Eastern Temperate Forests ecoregions. Anomalous records were detected for 20 reservoirs. Variables contributing to their detection were related to elevation characteristics (watershed and channel slopes, and minimum elevation), precipitation trends (maximum and cumulative monthly precipitation), dam properties (time since dam completion and initial trap efficiency), and CN. The detection of anomalies in an automated and fully-data driven way represents a powerful tool for the maintenance and monitoring of this large and heterogenous dataset with the potential of providing reliable information regarding the impacts of historical climate and watershed properties on erosion and sedimentation processes in US reservoirs.

Keywords: Reservoir sedimentation, reservoir capacity loss, machine learning, empirical data analytics, anomaly detection, multivariate analysis.

Practical Applications: The U.S. Army Corps of Engineers (USACE) created the Reservoir Sedimentation Information (RSI) system to compile historical reservoir elevation-capacity data collected using various measurement protocols, instruments, and analysis methods. These differences in data collection and analysis methods in addition to any human error can result in anomalies that require detection and correction before the dissemination of the dataset for further usage. Data anomalies are values that deviate from normal or expected patterns. Apparent erroneous data, related to duplicate records or increases in reservoir capacities, can be flagged through a preliminary analysis. However, the detection of anomalies in an automated and fully-data driven way represents a powerful tool for the maintenance and monitoring of this large and heterogenous dataset. A depurated RSI dataset is a potential major data source for large-scale and long-term studies related to sedimentation rates and suspended solid loads in freshwater systems due to the spatial and temporal scale of its records. This kind of dataset will allow the development of effective management plans for reservoir operation, maintenance, and upstream erosion control as well as enabling the indirect monitoring of suspended sediment loads in freshwater systems at a nationwide scale.

Introduction

Reservoirs and dams are fundamental components of the water resources infrastructure. supporting services such as water supply, flood risk control, hydropower generation, navigation, and recreation. The large life span of these structures (e.g., 100 years of operation (Pinson et al., 2016)) and their hydraulic characteristics make them susceptible to significant sedimentation processes. Consequences of sedimentation on reservoir functionality include capacity loss, water abstraction prevention due to buried intakes, navigability reduction, and damage to recreational areas. Moreover, uncertainties of U.S. reservoir operations are continuously rising as many are experiencing an increased frequency of extreme hydrologic events. This translate into increased maintenance costs that must be borne to recover reservoir functionality (Sholtes et al., 2018).

The analysis of historical survey information enables the assessment of aggradation trends, life expectancy, and reservoir vulnerabilities to climate change. This information is essential for the development of effective management plans for reservoir operation, maintenance, and upstream erosion control that include climate preparedness and resilience aspects. Considering the relevance of historical reservoir survey data for the nation's water resources, the U.S. Army Corps of Engineers (USACE) created the Reservoir Sedimentation Information (RSI) system to compile and assess data for over 700 dams primarily composed of elevation-capacity and elevation-surface area data derived from surveys.

The service length of USACE dams, most of them having more than 50 years, has a direct impact on the collected information. Data housed by the USACE RSI system entail multiple surveyors, measurement protocols, instruments, and analysis methods; therefore, differences are expected in the quality and quantities determined through periodic surveys. At times, these differences can result in anomalies that require detection and correction before being disseminated for further usage. Previous efforts conducted to detect hydrologic indicators for sedimentation processes based on USACE reservoir survey data identified inconsistencies in the dataset that impeded the accurate estimation of sedimentation rates (WEST Consultants, 2015). Due to the large number of reservoirs in the RSI system and the numerous parameters that influence sedimentation (e.g., watershed area, volume of water inflow, land use, and geologic characteristics), manual detection of data anomalies is a challenging, tedious, and costly task. Moreover, manual detection is limited to prior knowledge of the data and can skip anomalous records that are not easily identifiable in a large and multidimensional dataset.

Data anomalies are values that deviate from normal or expected patterns. More specifically, anomalies can be defined by deviation of observations from long-term averages in which the z-score (the number of standard deviations above or below the mean) outlier rejection test can be implemented for time-series products (Daszykowski et al., 2007). Anomalous data are also related to clustering processes (Gu and Angelov, 2017), in the sense that data either belongs to a global/local cluster or are considered rare records.

The detection of records that deviate from the normal or expected patterns in a dataset enables the flagging and possible identification of erroneous data, allowing the depuration of a dataset. Given the significant potential and uniqueness of the RSI dataset, identifying anomalous records will facilitate the extraction of meaningful information related to U.S. reservoirs and their basins.

A depurated reservoir sedimentation dataset will enable the development of indicators related to climate impacts on sedimentation rates, provide a comprehensive summary of USACE reservoir conditions, identify vulnerable reservoirs due to large sedimentation rates, assess the applicability of current and future data collection methods, and review methods and policies related to data collection (Minear and Kondolf, 2009; Pinson et al., 2016). Another potential application this dataset is the indirect monitoring of suspended sediment loads in freshwater systems, vital for channel and dam designing, water quality evaluation, hazard prediction, and ecosystem impacts assessment (Hazarika et al., 2020). Continuous measurements of suspended sediment from traditional in situ monitoring are difficult to obtain (Peterson et al., 2018), especially at a nationwide scale. The trap efficiency of large reservoirs, close to 100% (Brune, 1953; Ahmadi et al., 2019; Foster, 2020), allows the investigation of watershed processes such as erosion and suspended solid transport through reservoir sedimentation rate data.

In this study, data from 184 RSI reservoirs and associated watersheds features were analyzed to identify multivariate relationships within the dataset and anomalous records. A preliminary filtering was conducted to remove records with negative sedimentation rates and duplicate records. Subsequently, two unsupervised machine learning methods, the Autonomous Anomaly Detection (AAD) and the Kolmogorov-Smirnov and Efron (KSE) anomaly detection methods, identified likely erroneous data based on the multidimensional space and their relative location within the data cloud. Machine learning techniques are particularly useful in this dataset given the numerous parameters involved in erosion and sedimentation processes. Multivariate relationships and flagged records were then analyzed through the Principal Component Analysis (PCA) and the K-means clustering method.

Dataset development

Composite RSI Dataset Development

The composite RSI dataset was created with RSI reservoir sites that had three or more surveys and compiled variables related to sedimentation and hydrologic processes similar to Cox et al. (under review). The dataset was composed of records from 184 reservoirs located across the U.S. territory. Each record corresponded to a pair of subsequent surveys at a specific reservoir. For each record, the reservoir capacity loss was estimated as the difference of capacity between surveys for a single elevation. The maximum pool elevation not classified as a surcharge was used for the analysis. For reservoirs with no pool elevation, likely dry reservoirs, the spillway invert elevation was used.

In addition to the data for reservoir capacity loss between subsequent surveys, supplemental watershed data from publicly available data sources were compiled for each record to create the composite RSI dataset. The Application Programming Interfaces (APIs) in ArcGIS Pro and Google Colab were used to access, extract, and process data. The supplemental variables describing each record corresponded to topographic, climatologic, and other features relevant to watershed processes affecting erosion and sedimentation processes (Figure 1). Variables related to basin characteristics (e.g., latitude, longitude, area, slope, curve number, mean elevation mean, max elevation, etc.) and reservoir features (dam construction year, initial capacity, and initial trap efficiency) were assumed to be constant over time for a specific reservoir. The 42 selected variables for the composite dataset corresponded to identifiers (7), dates (3), categorical (2), and numerical (30) (categorical and numerical variables described in Table A- 1).

The location of reservoir drainage basins was specified through the average latitude and longitude extracted from the basin's shapefiles. The composite Curve Number (CN) and composite erodibility index values were computed as the area-weighted average for the corresponding drainage basin. The CN is an empirical hydrologic parameter that indicates the runoff potential of a catchment based its soil type and land use (USDA, 1986). CN maps for each basin, were created from national soil (Viger and Bock, 2014) and land cover (NLCD) (USGS, 2016) raster files. The soil hydrologic group and the land use category were the variables used to define the CN values according to USGS accepted table, as described in Tillman (2015). Erodibility index maps were developed following the technical guidelines of the Revised Universal Soil Loss Equation (RUSLE) (NRCS-USDA, n.d.) for each soil type. The average erodibility for sand (0.125), loam (0.325), and clay (0.1) were linked to the corresponding soil type on each basin soil map. The NLCD was also processed to compute the percentage of forested area in reservoir basins; deciduous, evergreen, and mixed forest were integrated in this analysis.

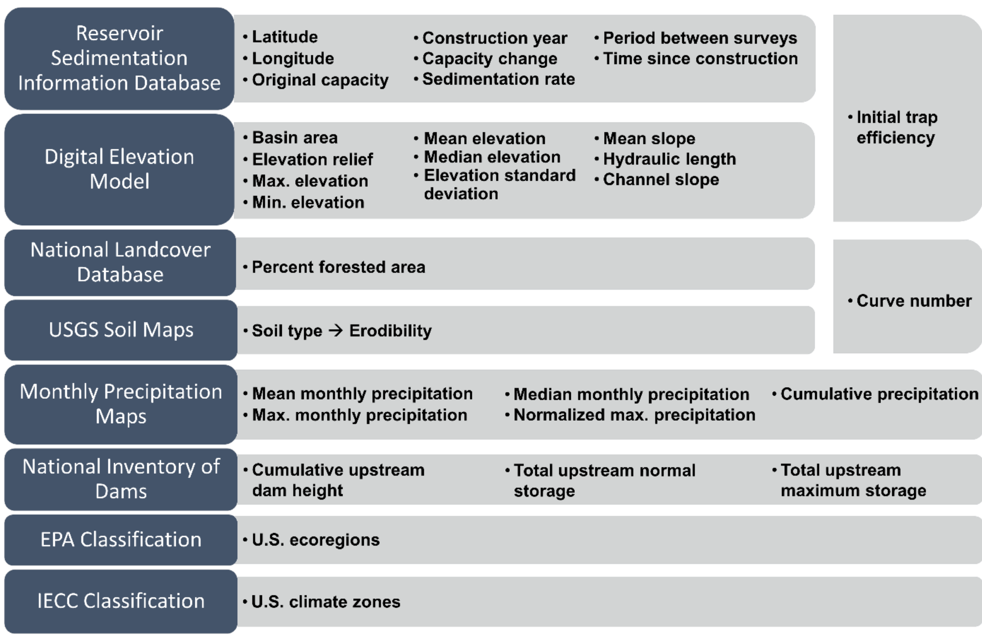

Figure 1. Data sources and derived variables (numerical and categorical) of the composite Reservoir Sedimentation Information (RSI) dataset.

A 1/3rd arc-second Digital Elevation Model (DEM) (USGS, 2017) was used to compute topographic related variables for the 184 reservoir drainage basins. Hydraulic length, basin elevation statistics, average slope, area, and relief, defined as the difference between maximum and minimum elevation, were calculated. The channel slope was then estimated as the relationship of basin relief over hydraulic length, and the initial trap efficiency (E) was computed with the original reservoir capacity (C) (m^3) and the reservoir drainage area (km^2) as described in (Brown, 1943; Garg and Jothiprakash, 2008):

$$E = 1 - \frac{1}{1+(2.1\times10^{-4})C/A} \quad (1)$$

The precipitation analysis for each drainage basin was conducted by analyzing 30 arc-second monthly precipitation raster files (Daly et al., 2015) corresponding to the time periods between each set of consecutive surveys. The analysis computed cumulative, maximum monthly, mean monthly, and median monthly precipitation for each one of the records. The normalized maximum precipitation was computed as the ratio of the maximum and the mean monthly precipitation.

Given the large number of dams built upstream of RSI reservoirs, a batch analysis was conducted to include upstream dam's height and storage. Two main steps were executed: initially, the National Inventory of Dams (NID) dataset (USACE, n.d.), composed of over 90,000 U.S. dams, was used to create yearly time series of cumulative upstream dam height, and normal and maximum storage for each RSI reservoir; subsequently, the upstream dam variables were time averaged for the period comprised between two subsequent surveys of each RSI dataset record.

Finally, the categorical variables of US Environmental Protection Agency (EPA) ecoregion (Figure A- 1) and IECC climate zone (Figure A- 2) were included, having 10 and 7 categories within the conterminous U.S. territory, respectively. The EPA ecoregions are areas having similar ecosystems, identified through the biotic, abiotic, terrestrial, and aquatic components. Ecoregions are fundamental for the implementation of management strategies (EPA, n.d.). Alternatively, the IECC climate zones are used to identify regions with similar requirements on heating/colling, mechanical, lighting, and water heating systems for buildings based on climate conditions (Office of Energy Efficiency & Renewable Energy, n.d.). The category assign to each record was the prevalent one in the basin's area.

Dataset Pre-processing

Reservoir capacity is expected to decrease over time as the physics of natural processes make sustaining or increasing reservoir capacity not possible unless specific maintenance projects are conducted, such as dredging or free flow flushing (Wang and Hu, 2009). Based on the nature of the data within the RSI composite dataset and the knowledge about the physical meaning of its variables, a preliminary filtering process was developed to remove evident erroneous data: Records corresponding to a set of consecutive surveys having identical survey dates, identical consecutive capacities, or increases in capacity.

Given the variety of information contained in the composite RSI dataset, significant heterogeneity in the order of magnitudes, scales, and units is expected (Table A- 1). Preliminary results demonstrated that variable scale discrepancies and zero values impacted the performance of the automated anomaly detection. Data transformation and normalization techniques were applied to the composite dataset to reduce the bias from records having relatively large or zero values. A *log(x+1)* transformation (Brakstad, 1992; Emmerson et al., 1997) was applied to the numerical variables to remove the impact of the difference between orders of magnitude (for reference see minimum and maximum values in Table A- 1). Subsequently, the min-max normalization (Goyal et al., 2014; Patro and Sahu, 2015) was implemented to fit the data in a pre-defined range keeping the relationships from original data unchanged (Patro and Sahu, 2015). The log-transformed data were linearly normalized to a 0.15 to 0.85 scale. The obtained dataset was used in all the methods described hereafter. Data transformation and preprocessing have been widely used to improve the performance of ML methods (Jiang et al., 2008; Ahmed et al., 2010; Kocaguneli et al., 2012; Huang et al., 2015; Meharie and Shaik, 2020)

Automated Analysis Methods

Unsupervised learning techniques were implemented to analyze the dataset. A Principal Component Analysis (PCA) was initially conducted to explore and visualize the variability of the dataset and analyze relationships existing between variables. Subsequently, the Empirical Data Analytics (EDA) based method (i.e., Autonomous Anomaly Detection, AAD) and the Kolmogorov-Smirnov and Efron Anomaly Detection method were performed. Results were visually analyzed by plotting flagged records in the principal component (PC) dimensions and by mapping reservoirs with flagged records.

Principal Component Analysis (PCA)

PCA is a multivariate and statistical method frequently applied to interpret the variability of large environmental datasets, offering major advantages over univariate analyses (Reid and Spencer, 2009). The main advantage of the PCA technique is the dimensionality reduction of the dataset (Martinez and Kak, 2001), which is achieved by creating new uncorrelated variables, called Principal Components (PCs), that maximize the variance of the dataset, preserving most of its information (Jolliffe and Cadima, 2016). As a descriptive tool (as opposed to inferential), PCA does not require the data to follow any distribution to be applied. The math behind this method consists of creating the PCs as linear combinations of the original variables that maximize the variance, this is equivalent to solving the eigenvalues and eigenvectors of the covariance matrix. The eigenvalues correspond to the variances of the linear combinations defined by the corresponding eigenvectors, or PCs (Jolliffe and Cadima, 2016). The resulting PCs axes are orthogonal and sorted according to their variance. The PCA space is described in Eq. (2), where matrix X holds the original records in the multidimensional space, P is the matrix of the PCs space and holds the contributions of variables to each PCs, and S contains the records' scores projected in the PC space.

$$XP = S \tag{2}$$

The number of PCs needed to adequately describe the dataset and analyze its variability is usually smaller than the original number of variables, facilitating the interpretation and visualization of data. In addition, the loading matrix P allows for the analysis of correlations between variables (Aguado et al., 2008).

A PCA was run in the MATLAB software with the 30 transformed and normalized numerical variables. The variance and the variables' contribution for each PCs were analyzed. In addition, the projection of all records was plotted in the space of PCs holding the largest variance. This provided a visualization of the dataset prior to the anomalous detection analysis, as well as the records flagged as anomalous in the dataset.

Autonomous Anomaly Detection (AAD)

This technique is a novel application of artificial intelligence on anomaly detection for reservoir sedimentation datasets. Based on Empirical Data Analytics (EDA), the AAD is a nonparametric, fully data-driven, unsupervised method. In other words, this method does not require user-defined thresholds to identify anomalies, which represents a great advantage compared to supervised methods as variable thresholds can be different by region or even by specific reservoir. The EDA framework utilized in this project, first proposed by Angelov et al. (2016), applies three non-parametric estimators: cumulative proximity, unimodal density, and multimodal density to identify local anomalies from data clouds (Angelov et al., 2016; Gu and Angelov, 2017). The cumulative proximity of a record ($Q(x_i)$) is the summation of the square distances (d^2) to all the other points in the dataset (Angelov et al., 2016; Peterson et al., 2020):

$$Q(x_i) = \sum_{j=1}^{K} d^2\left(x_i, x_j\right), i = 1,2, \dots, K \tag{3}$$

The unimodal density (D) represents the relationship of a data point with the "tail" of the data distribution (Angelov et al., 2016) and it represents the inverse of the standardize eccentricity (ε):

$$D(x_i) = \varepsilon^{-1}(x_i) = \frac{E[Q(x)]}{2Q(x_i)}, i = 1,2, \dots, K \tag{4}$$

Where $E[Q(x)]$ is the expected value of the cumulative proximity:

$$E[Q(x)] = \frac{1}{K}\sum_{i=1}^{K} Q(x_i) \tag{5}$$

Finally, the multimodal density is the unimodal density weighed by the frequency of occurrence (Peterson et al., 2020) which has the capability of exposing local modes of the data distribution. Understanding that x_i denotes one record from the total amount of records K in the dataset, and u_j denotes a unique record with a corresponding frequency f_j in the dataset such that the summation of frequencies for all u_j equals K, the multimodal density value of a unique record u_j is:

$$M\left(u_j\right) = f_j D(u_j) \tag{6}$$

The AAD method initially identifies potential anomalies by applying the mentioned estimators, then it forms clusters from the potential anomalies to evaluate the existence of local anomalies. This EDA-based method successfully identifies anomalies from the mutual distribution of the data within the data space and the ensemble properties (Gu and Angelov, 2017). The AAD approach has been compared to the "3σ" method (Thomas and Balakrishnan, 2009), and the anomaly detection through random walks (ODRW) method (Moonesinghe and Tan, 2006) resulting in a more accurate and objective method, suitable for the identification of global and local anomalies (Angelov et al., 2016; Peterson et al., 2020). The output from this method, a vector containing potential anomalous records, was used along with the PCs axes to identify the location of these records within the data cloud.

Kolmogorov-Smirnov and Efron (KSE) Anomaly Detection Method and Z-Score

The KSE anomaly detection method is based on the Kolmogorov-Smirnov (KS) statistical test and the Euclidean distance (EUD) between data points (Jirachan and Piromsopa, 2015). The KS test compares two datasets and returns a score between 0 and 1 that indicates the similarity of the dataset's distribution functions (DFs), such that a high value indicates a likely anomaly. In the KSE method, random resampling is employed to generate pairs of empirical DFs of EUD, which are then evaluated with the KS test. Having a dataset D, random subsamples S_1 and S_2 with n number of records each, are created. Thereafter, two DFs are created, DF_i corresponding to the DF of EUDs from a point p_i in D, to each point in S_1, and DF_j corresponding to the DF of EUDs from point p_j in S_2, to all data points in S_1. The KS statistic between point p_i, in D, and any point in S_2 is computed as follows:

$$KS(p_i, p_j) = Max\left|DF_i - DF_j\right| \tag{7}$$

Finally, the average of the KS statistics for all p_j in S_2 is defined as the KSE statistic for point p_i (Jirachan and Piromsopa, 2015):

$$KSE(p_i) = \frac{1}{n-1}\sum_{j=1\ j\neq i}^{n} KS(p_i, p_j) \tag{8}$$

The output from this method is a vector containing the KSE scores for all the records in the dataset.

To achieve an objective analysis of the obtained KSE scores, the Z-score method was chosen to estimate a threshold score for anomalous data. The Z-score Eq. (9) is an indicator of the location of a record with respect to the mean and it is measured in terms of standard deviations. A record with a Z-score of two is located two standard deviations apart from the mean. From a percentile approach, a record having a Z-score greater than two signifies that it is larger than 97.7% of the records in the dataset. A Z-score of two was chosen as threshold for analyzing the obtained KSE-scores.

$$Z - score = \frac{x_i - \mu}{\sigma} \tag{9}$$

where x_i is the record *i* of variable *x*, μ is the mean of variable *x*, and σ is the standard deviation of variable *x*.

K-means Clustering Algorithm

This unsupervised clustering algorithm was used along with the PCs dimensions to analyze the results from the AAD and the KSE methods. The K-means method categorizes data into clusters by iteratively locating cluster centroids and computing the Euclidean distances from data points to the centroids. On each iteration the centroids are recalculated by computing the mean of cluster data points (Jirachan and Piromsopa, 2015). The average silhouette (Rousseeuw, 1987) and the Davies Bouldin (Davies and Bouldin, 1979; Bolshakova and Azuaje, 2003) methods were used for the selection of the optimum number of clusters.

RESULTS AND DISCUSSION

The RSI composite dataset initially contained 622 records from 184 reservoirs. Three variables (Total Upstream Max Storage, Total Upstream Normal Storage, and Total Upstream Dam Height) had missing data, not exceeding 13 records, that were replaced with the mean for the corresponding variable. The prior-knowledge filtering identified 155 records corresponding to sets of consecutive surveys having: the same survey data, identical dates, identical capacities, or an increasing trend on the capacity. These records were filtered out from the dataset, which finalized with 467 records from 174 reservoirs (Figure 2). Maximum, minimum, and mean values of numerical variables for the resulting dataset are reported in Table A- 1. Inconsistencies in reservoir sedimentation data related to increases in reservoir capacity were also identified in a previous study of the RSI database (WEST Consultants, 2015). These inconsistencies are linked to the considerable temporal extent covered by RSI composite dataset. Surveys performed at different times will likely use different technologies and analysis methodologies, as sciences and engineering create new and updated instruments.

The PCA was performed with the transformed and normalized numerical variables of the composite RSI dataset. The percentage of variance held by PC1-PC4 was 42.1, 16.7, 9.6, and 7.2, respectively (Table 1). This means that an analysis containing these four PCs would carry 75.7% of the variance present in the initial dataset. The analysis of PCA results based on 75% or less of its total variance has been implemented in varied fields of study (Derbew, 2020; Chiomento et al., 2021), with an acceptable minimum of 60% of variance (Dumicic et al., 2015). The relatively broad distribution of the variance among multiple PCs (e.g., most of the variance not being exclusively held by 1st and 2nd PCs) reveals the relatively low redundance in the dataset information. The contribution of variables to PC1-PC4 was examined discerning positive and negative PC directions.

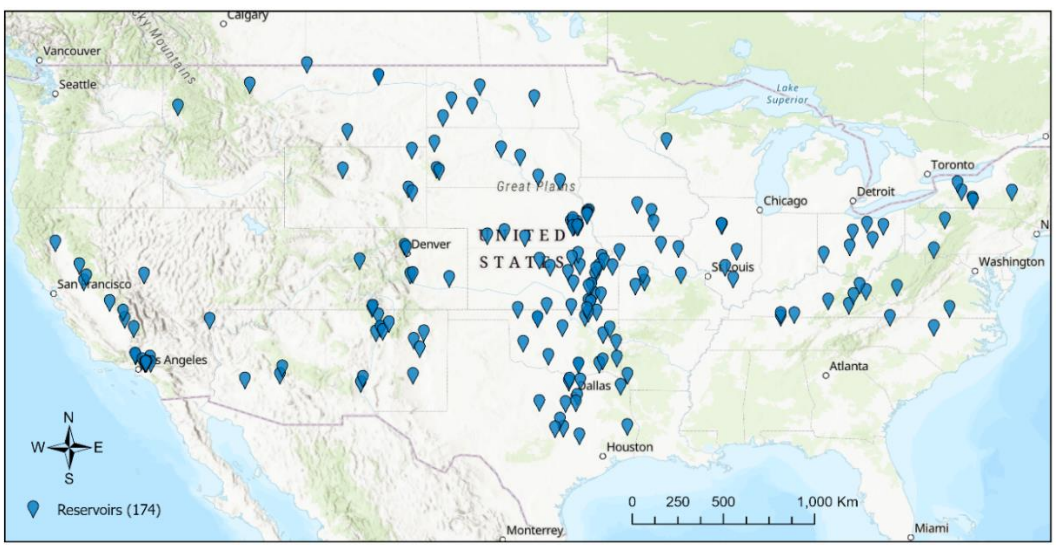

Figure 2. Location of the 174 reservoirs of the RSI composite dataset.

The PCA loading plots (Figure 3) indicate the importance of each variable to the analysis. The length of the variable vector indicates its impact in the PCA. In the same way, the orthogonal components of a variable vector indicate its contribution to the corresponding PCs. Variables with the greatest contributions for PC1-PC4 are presented in Table 1. The variables having the most significant contributions to +PC1 were those related to drainage basin elevation characteristics, namely: maximum elevation, elevation relief, elevation standard deviation, and elevation mean and media (Table 1). The +PC2 was defined by variables related to dam properties and basin extent, such as original capacity, basin area, hydraulic length, sedimentation rate, total upstream normal storage, capacity loss, total upstream dam height, and total upstream maximum storage; for +PC3 the greatest contribution was obtained from the percentage of forested area with lower contributions of variables measuring precipitation central tendency (mean and median); +PC4 was mainly influenced by variables related to extreme precipitation events such as normalized maximum precipitation, and maximum precipitation, while -PC4 was mainly contributed by geo-location variables (latitude, longitude) and minimum elevation.

The relative location of variable vectors within the PC space (Figure 3) was analyzed to reveal existent relationships between variables. Even though reservoirs having large drainage areas (BA) also have relatively large upstream reservoir storage capacity (UpsNorSt), they are expected to have large sedimentation rates (SedRt) and subsequent capacity losses (CapLoss) (Figure 3a). This might also be influenced by the impact of runoff rates in these basins. The CN makes a lesser but still important contribution to PC2. Hence, large basins, with potentially high runoff rates will trigger erosion and transport processes that exceed upstream storage capacities and impact downstream reservoir storage. Although sediment trapping by upstream reservoirs has been reported to have a significant impact on downstream capacity losses (Minear & Kondolf, 2009), and upstream reservoir storage is certainly related to upstream sediment trapping, as the former limits the latter, only the change in upstream storage over a period of time would accurately estimate the trapping occurring in upstream reservoirs. Alternatively, the relationship between basin area and sediment yield to reservoirs has been largely identified (Walling, 1983; Richards, 1993; Avendaño Salas et al., 1997; Lu et al., 2005). In fact, there is a mathematical formulation that estimates sediment yield from the drainage area. The sediment delivery ratio is computed as $kA^{-0.125}$ where k is a constant depending on the location, and A is the basin area (American Society of Civil Engineers, 1975; Graf et al., 2010). Although other expressions have related sediment delivery ratios to other physical variables, drainage area remains the most significant one (Graf et al., 2010). Basin elevation properties (DEMMax, DEMMed, DEMMean) and relief (BaRlf) were found to have little incidence in the sedimentation rates and capacity losses of reservoirs. In other words, reservoirs in the RSI composite dataset showed a variety of sedimentation rates and capacity losses for the entire range of elevation related variables, for which there is not a conclusive relationship between them. Regarding precipitation related variables, basins located in southern regions (small AvLat) experienced larger extreme events (NormPre, MaxPre), while basins with extensive, forested areas (Forest) had higher values of average precipitation (MedPre, MeanPre) (Figure 3b). No relationship was found between percentage of forested area and values of maximum precipitation.

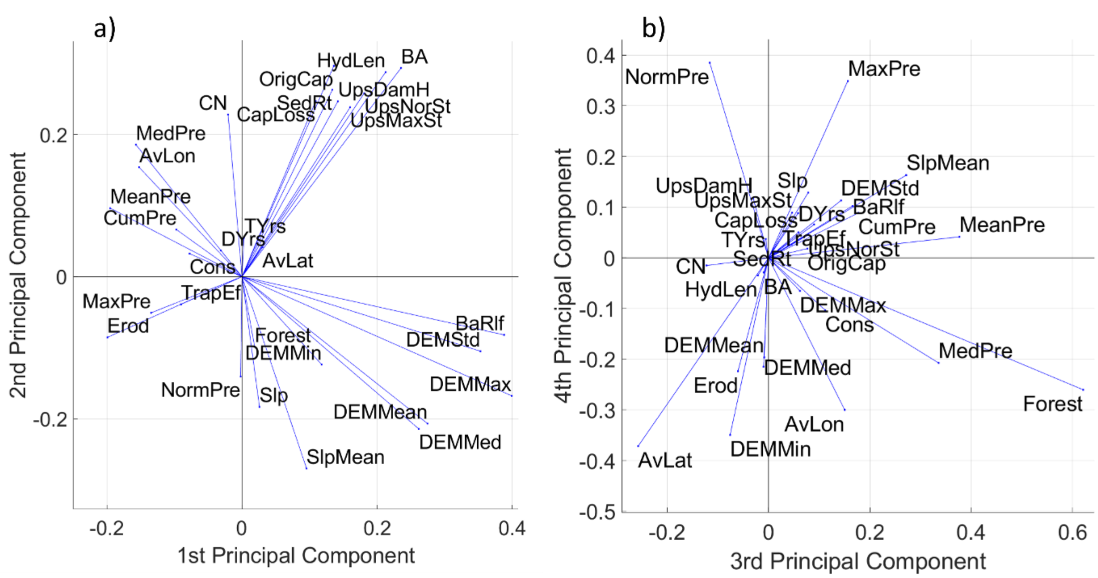

Figure 3. Plot of variable loads for Principal Component (PC) 1-PC4. a) PC1 vs. PC2, b) PC3 vs. PC4. See Table A- 1 for variable abbreviations references.

The PCs' space was used to visualize the records in the multidimensional dataset and analyze the connection between categorical and numerical variables. Clusters and record location in the PC space provide information regarding the associated values for the numerical variables which are extracted from the variable loads for each PC (Figure 3, Table 1). Regarding EPA ecoregions, some categorical clusters were clearly differentiated and opposed by the PCs (Figure 4a and c). Records from Eastern Temperate Forests, located in the left side of PC1, had smaller values of elevation related variables than records from the Northwestern Forested Mountains and North American Desserts. As expected, clusters from Eastern Temperate Forests and Northwestern Forested Mountains categories were nearly identically located in the positive direction of PC3. Meaning that the mentioned ecoregions have large values for the forested areas and average precipitation variables. The location of these two ecoregions in the PC space also indicated a wide range of values for maximum precipitation and geo-location related variables. Records pertaining to the Mediterranean California ecoregion were clearly localized in the negative direction of PC2 and the positive direction of PC4, which indicated low values of capacity loss, sedimentation rate, basin area, CN, and latitude, and large values of maximum precipitation. This suggested that, although reservoirs located in the Mediterranean California experienced substantial extreme precipitation events, their small basin areas and low CN values were reflected in low capacity losses for the associated reservoirs. In general terms, records having larger reservoir capacity loss and sedimentation rate were either from the Great Plains or the Eastern Temperate Forests ecoregions, while Mediterranean California and Northwestern Forested Mountains had smaller capacity losses.

The IECC climate zone clusters did not show any separation or opposition of categories in the PC1 vs. PC2 space (Figure 4b). This outcome is explained by the fact that the variables contributing to these PCs are indicators of basin extent and elevation, as well as reservoir properties, which are not related to climate classification criteria. On the contrary, PC4 (Figure 4d) showed a gradation of clusters from top to bottom, with the climate zones 2, 3, and 4 in the positive PC4 direction, and 5, 6 and 7 in the negative PC4 direction. PC4 main contributing variables are maximum precipitation and eco-location related variables, which indicates that records from climate zones 2, 3, and 4 in the southern regions and have large extreme precipitation events, while zones 5, 6, and 7, located in the northern regions, have small values of maximum precipitation. The geolocation of clusters from the PCA analysis agrees with the geographic distribution of climate zones across the conterminous U.S. (Figure A- 2).

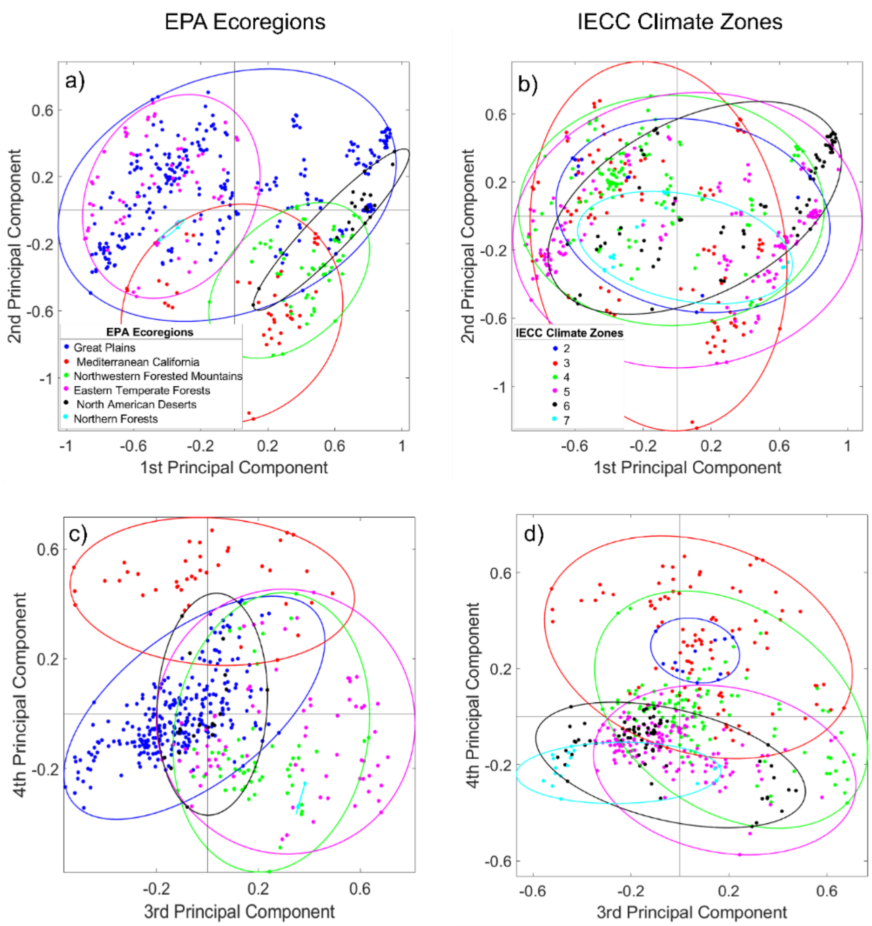

Figure 4. Records classified by US Environmental Protection Agency (EPA) ecoregions on a) PC1 vs. PC2 and c) PC3 vs. PC4, respectively; records classified by IECC climate zone on b) PC1 vs PC2 and d) PC3 vs PC4, respectively.

After analyzing the variables and records housed by the RSI composite dataset, anomaly detection methods were applied. The AAD method flagged 18 records as potential anomalous data, corresponding to 15 reservoirs (Table 2). Anomalous records corresponded to reservoirs located in the Mediterranean California, Eastern Temperate Forests, Northwestern Forested Mountains, and North American Desserts and climate zones ranging from 2 to 6. For the KSE method, the scores for all the records ranged from 0.18 to 0.77 (Figure 5). The Z-score method was applied to the KSE-scores to estimate a threshold value to flag potential anomalies. A KSE-score of 0.4 was found to correspond with a Z-score of two, being larger than 97.7% of the computed KSE-scores. With this threshold, 15 records were flagged as anomalous, corresponding to 10 reservoirs (Table 2). These were located in the Mediterranean California, the Great Plains, and the Northwestern Forested Mountains, with climate zones 3,4 and 5. Reservoirs 2, 9, 100, 169, and 182 had records flagged for both AAD and KSE methods (Figure 6). These reservoirs were in the Mediterranean California and the Northwestern Forested Mountains, and climate zones 3 and 5.

The projection of data on the PCs space was used to visualize the records flagged as potentially anomalous. To explore possible clusters and the location of the anomalies with respect to clusters, the K-means algorithm was applied to the data. Results from the average silhouette and the Davies Bouldin methods suggested two clusters as the optimum number of clusters for the RSI composite dataset. The identified clusters were plotted in the PCs space along with the flagged records (Figure 7). It was evident that the K-means cluster analysis was dominated by the PC1 (Figure 7a), with clusters being opposed by this axis. Some anomalous data appeared to lie on cluster edges (Figure 7a) indicating that variables contributing to the corresponding PC (Table 1) may also be contributing to the flagging of these records. However, other flagged records appeared to be within the respective clouds of data (Figure 7). This suggested that, for this dataset, other variables different than those with high contributions to PCA axes might be triggering the detection of certain anomalous records.

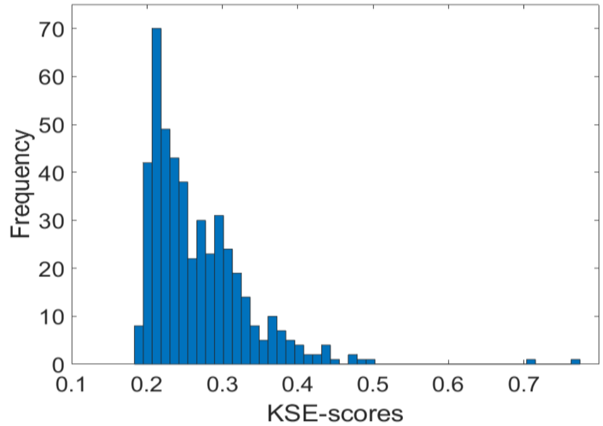

Figure 5. Histogram of the KSE-scores estimated for all records.

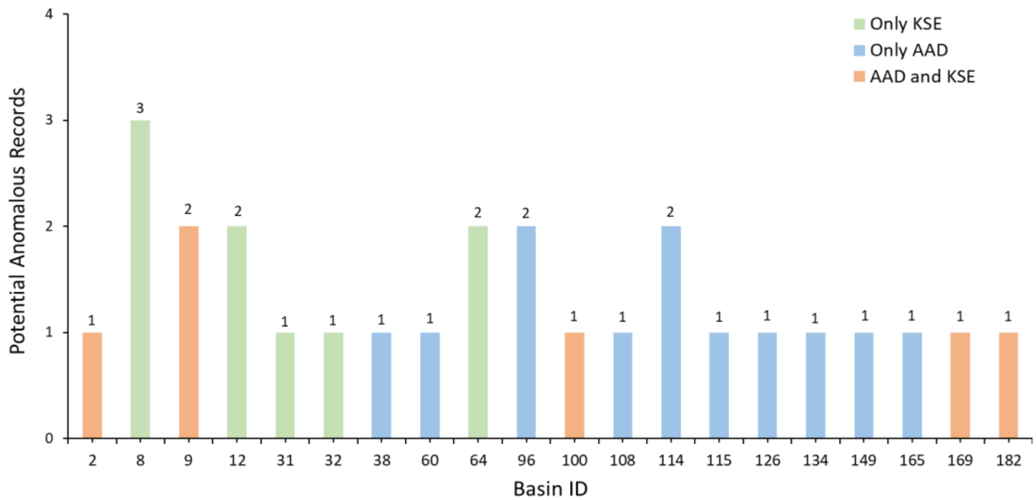

Figure 6. Count of potential anomalous records detected by the AAD and KSE methods per reservoir's basin.

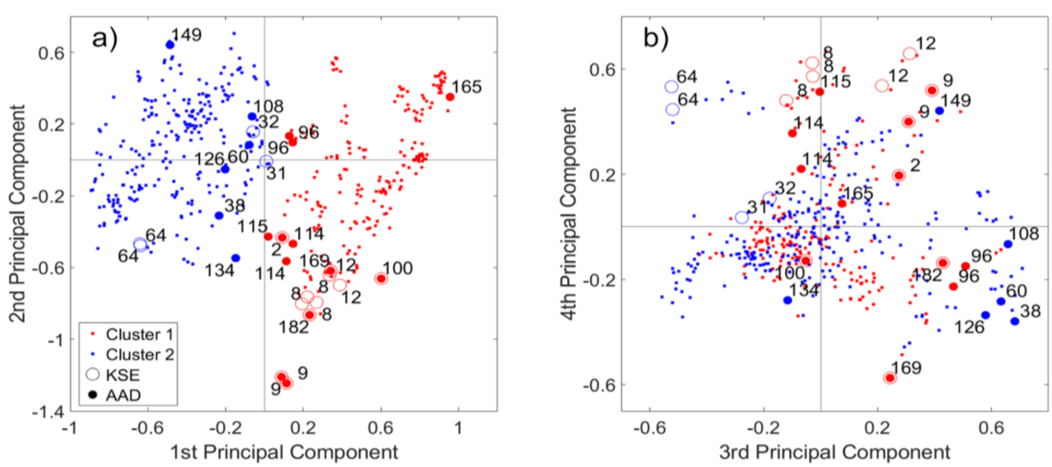

Figure 7. K-means clusters plotted in the a) PC1 vs. PC2 and b) PC3 vs. PC4 dimensions. Anomalous records flagged by AAD and KSE methods are specified by marker and labels correspond to Basin ID number.

While the PCA loads identify the variables causing the largest global variability for the entire dataset, the AAD and KSE methods analyzed the relative location of each record within the multidimensional space. Variables with the largest variation within the entire data cloud (high loads for PCA) might not be the main triggers to indicate anomalous records. In other words, the variables triggering the anomaly detection likely have similar values for most records, with the anomalous ones as outliers. The following single-variable outlier analysis for anomalous records using Z-scores values was conducted to further identify the main variables causing ML methods to flag records. Scatter plots of normalized variables outside the *mean +/- standard deviation* fringe for all anomalous records were analyzed (Figure 8 and Figure 9).

All records detected as anomalous by the AAD method had at least one variable with a Z-score larger than two, while two anomalous records detected by KSE method (corresponding to basins 31 and 32) did not exhibit variables with Z-scores larger than two. These two records also had the lowest KSE-scores, which suggests that the KSE threshold value for identifying anomalous data could be increased from the selected 0.4 value, and that these two records may not be anomalous. Among all the variables, the channel slope values (Slp) had notably large Z-scores in a couple of records, Slp values were 5 and 7 standard deviations apart from the mean for basins 182 and 9, respectively. Records from these basins were flagged by both AAD and KSE methods, and basin 9 records had the largest KSE-scores. Figure 8 and Figure 9 organized variables from high to low cumulative covariance on its horizontal axis. Those with the largest cumulative covariance (towards the left side) matched the most relevant variables on the PC loads analysis as they provide the larger global variability for the whole dataset. Conversely, variables located towards the right side (low cumulative covariance) included those with the largest Z-scores for anomalous records, having most of their values clustered towards the mean with a few outlier values corresponding to the anomalous records. This is the case of Slp, one of the variables with the smallest *mean +/- 2 standard deviation* fringe, and with values for basins 9 and 182 in the farthest upper range. Other variables with significantly large Z-scores for anomalous records (close to four) were related to elevation characteristics (SlpMean and DemMin), precipitation trends (NormPre, MaxPre and CumPre), dam properties (TYrs and TrapEf), and hydrologic properties (CN).

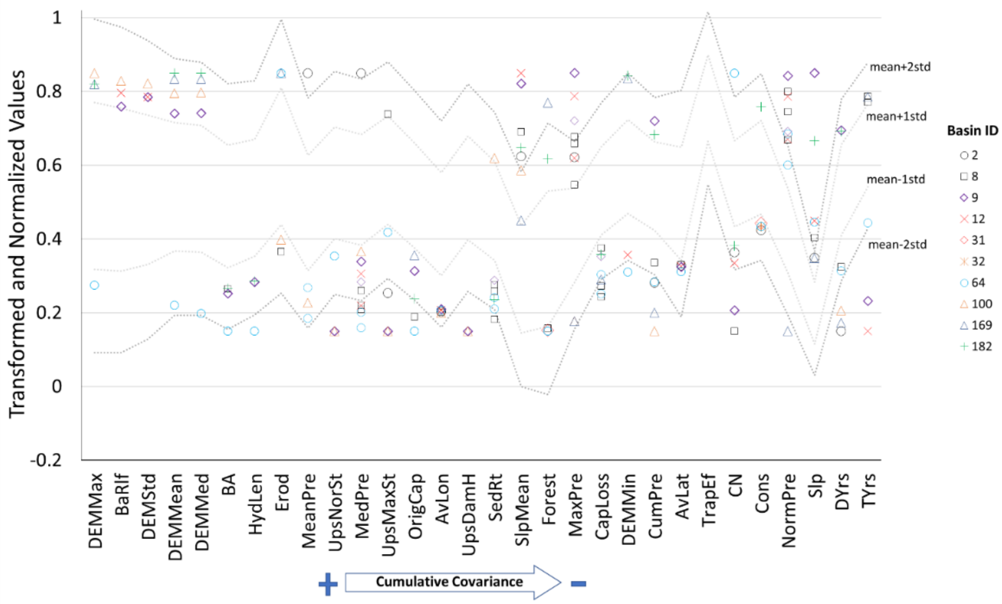

Figure 8. KSE anomalous records with values outside *the mean +/- standard deviation* fringe.

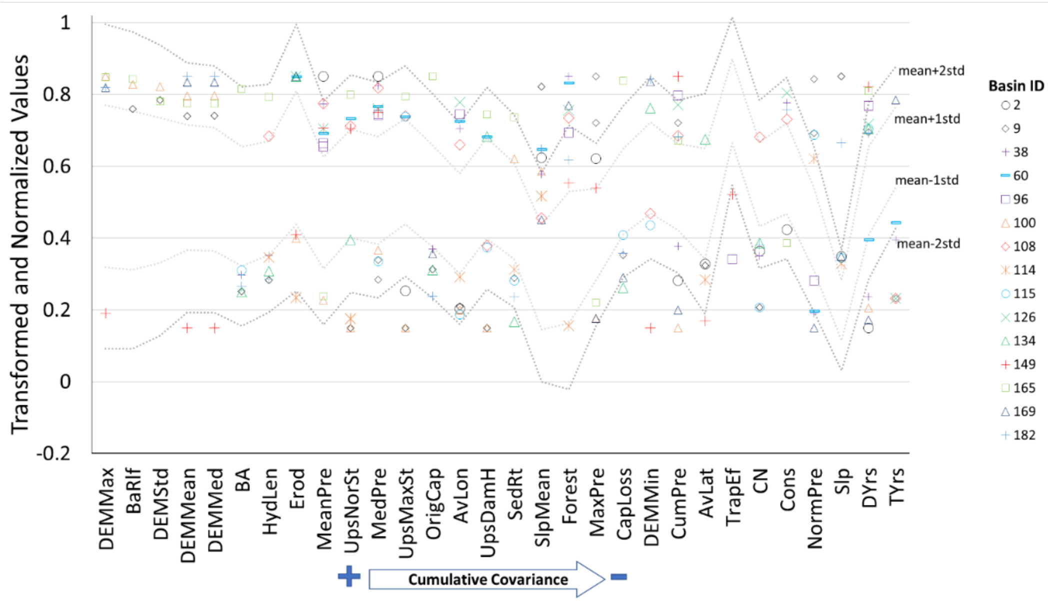

Figure 9. AAD anomalous records with values outside the *mean +/- standard deviation* fringe.

CONCLUSIONS

This study performed a multivariate analysis, diagnosis, and interpretation of a composite dataset of reservoirs sedimentation and associated watersheds parameters. Prior-knowledge filtering, two machine learning techniques, AAD and KSE, and a multivariate analysis, PCA, were used to identify likely erroneous data, as well as investigate relevant information and relationships within this unique dataset. This research highlights the challenges related to data analysis and depuration of datasets containing physical variables of heterogeneous nature. Raw values facilitated the initial prior-knowledge based filtering but data transformation techniques were required for the automatic detection of anomalous records to remove the bias introduced by scale differences and null values.

Variables holding most of the data cloud variance were grouped by the PCA as follows 1) basin topographic features, 2) dam properties and basin extent, 4) forested area and average precipitation, and 5) geo-location descriptors and maximum precipitation. PCA loading plots indicated that sedimentation rates and capacity losses in the reservoirs were mainly related to drainage basin size and potential runoff processes, while being independent of elevation related properties. EPA ecoregions with larger reservoir capacity losses either belonged to the Great Plains or the Eastern Temperate Forests, as opposed to Mediterranean California and Northwestern Forested Mountains having the smaller capacity losses.

The anomaly detection methods flagged 20 reservoirs for having anomalous records. The flagged records should be analyzed and verified by managers and operation staff and handled with caution by RSI dataset users. Variables potentially causing these records to be flagged were related to elevation characteristics (Slp, SlpMean, and DemMin), precipitation trends (NormPre, MaxPre and CumPre), dam properties (TYrs and TrapEf), and watershed properties (CN).

Further development of the RSI composite dataset could consider the addition of other watershed variables that can potentially influence sedimentation and erosion processes. Mean and maximum streamflow, and percentage of agricultural land, could provide new information associated to soil particle detachment and transport processes. In addition, the normalization of capacity loss and sedimentation rate by the basin area could enable the identification of further relationships within the dataset.

APPENDIX

Table A- 1. Numerical and categorical variables included in the dataset. Mean, maximum, and minimum values computed from original dataset (before transformation and normalization).

Abbreviation	**VARIABLE NAME (UNITS)**	**TYPE**	**MEAN**	**MIN**	**MAX**
AvLat	Average Watershed Latitude	Numerical	38.7	30.4	49.0
AvLon	Average Watershed Longitude	Numerical	-1.01E+02	-1.23E+02	-75.2
BA	Basin Area (km^2)	Numerical	4.94E+04	1.25E+01	7.21E+05
BaRlf	Elevation Relief (m)	Numerical	1.25E+03	5.16E+01	4.19E+03
CapLoss	Capacity Loss (m^3)	Numerical	3.18E+07	1.23E+03	1.65E+09
CN	Curve Number	Numerical	73.4	53.8	92.0
Cons	Construction Year	Numerical	1.96E+03	1.91E+03	1.99E+03
CumPre	Cumulative Precipitation (cm)	Numerical	1.07E+03	4.66E+01	6.65E+03
DEMMax	Maximum Elevation (m)	Numerical	1.79E+03	1.96E+02	4.41E+03
DEMMean	Mean Elevation (m)	Numerical	9.16E+02	1.03E+02	2.85E+03
DEMMed	Median Elevation (m)	Numerical	8.79E+02	1.03E+02	2.80E+03
DEMMin	Minimum Elevation (m)	Numerical	5.42E+02	1.55E+01	2.18E+03
DEMStd	Elevation Std (m)	Numerical	2.23E+02	8.25E+00	8.65E+02
DYrs	Duration of Period Between Surveys (yrs)	Numerical	14.5	0.75	65.1
Erod	Erodibility	Numerical	0.25	0.10	0.33
EPA	EPA Ecoregion	Categorical	-	-	-
Forest	% Forested Area	Numerical	0.22	0.00	0.91
HydLen	Hydraulic length (m)	Numerical	4.84E+05	6.81E+03	3.86E+06
IECC	IECC Climate Zone	Categorical	-	-	-
MaxPre	Max. monthly precipitation (mm)	Numerical	249.43	81.53	1040.38
MeanPre	Mean Monthly Precipitation (mm/mo.)	Numerical	60.45	22.35	133.86
MedPre	Median Monthly Precipitation (mm/mo.)	Numerical	48.51	3.81	118.11
NormPre	Normalized Max. Precipitation	Numerical	4.27	1.56	13.6
OrigCap	Original Capacity (m^3)	Numerical	1.88E+09	9.33E+05	4.02E+10
SedRt	Sedimentation Rate (m^3/yr)	Numerical	3.00E+06	1.85E+02	1.67E+08
Slp	Channel Slope	Numerical	0.01	0.00	0.10
SlpMean	Mean Slope (m/m)	Numerical	0.11	0.01	0.55
TrapEf	Initial Trap Efficiency	Numerical	0.90	0.17	1.00
TYrs	Time Since Construction (years)	Numerical	23.5	-3.00	93.0
UpsDamH	Total Upstream Dam Height (m)	Numerical	2.81E+03	0.00E+00	5.02E+04
UpsMaxSt	Total Upstream Max Storage (m^3)	Numerical	9.17E+09	0.00E+00	1.88E+11
UpsNorSt	Total Upstream Normal Storage (m^3)	Numerical	6.34E+09	0.00E+00	1.41E+11

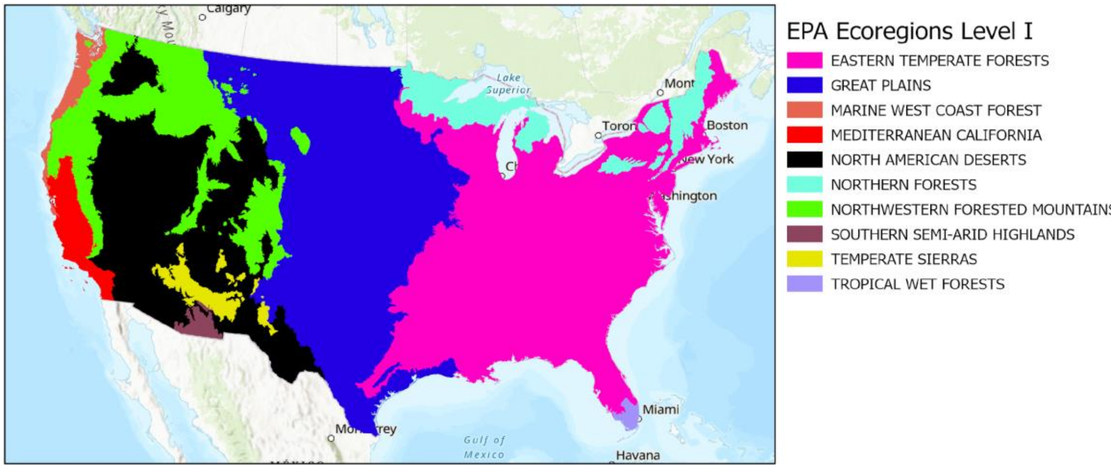

Figure A- 1. EPA Level 1 Ecoregions (Adapted from EPA, n.d.-a).

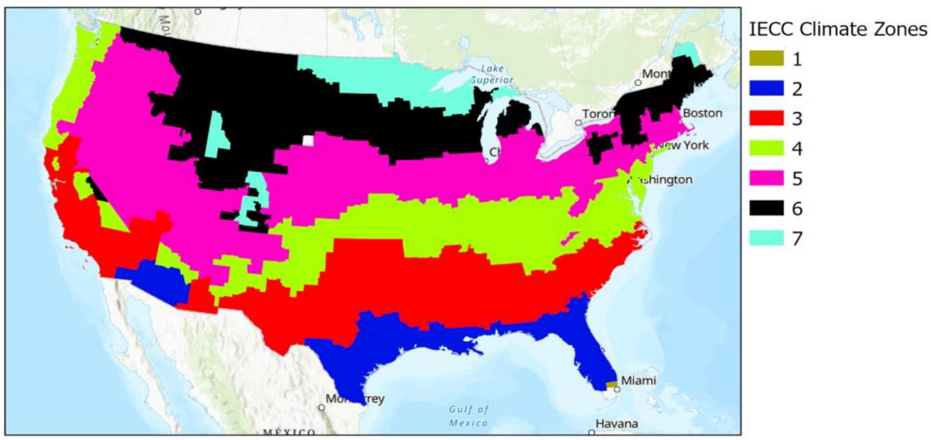

Figure A- 2. IECC Climate Zones (Adapted from U.S. Energy Information Administration, 2020).

DATA AVAILABILITY

Data from the USACE RSI system are not currently publicly available. The USACE is conducting quality control of the database and plans to publicly release the data following completion of that effort. Watershed related data were derived from publicly available resources cited accordingly in the Dataset Development section.

ACKNOWLEDGEMENTS

This research was supported by the U.S. National Science Foundation (Award # 1948940) and the WATER Institute at Saint Louis University.

REFERENCES

Aguado, D., Montoya, T., Borras, L., Seco, A. & Ferrer, J. (2008) Using SOM and PCA for analysing and interpreting data from a P-removal SBR. *Engineering Applications of Artificial Intelligence,* 21(6)**,** 919-930. 10.1016/j.engappai.2007.08.001.

Ahmadi, A., Zolfagharipoor, M. A. & Afzali, A. A. (2019) Stability Analysis of Stakeholders' Cooperation in Inter-Basin Water Transfer Projects: a Case Study. *Water Resources Management,* 33(1)**,** 1-18. 10.1007/s11269-018-2065-7.

Ahmed, N. K., Atiya, A. F., El Gayar, N. & El-Shishiny, H. (2010) An Empirical Comparison of Machine Learning Models for Time Series Forecasting. *Econometric Reviews,* 29(5-6)**,** 594-621. Pii 926963705 10.1080/07474938.2010.481556.

American Society of Civil Engineers (1975) Sedimentation engineering, Manuals Rep. Eng. Practice 54. New York.

Angelov, P., Gu, X., Kangin, D. & Principe, J. Empirical data analysis: A new tool for data analytics. *2016 IEEE International Conference on Systems, Man, and Cybernetics (SMC)*. 9-12 Oct. 2016. 000052-000059.

Avendaño Salas, C., Sanz Montero, M. E., Cobo Rayán, R. & Gómez Montaña, J. L. (1997) Sediment yield at Spanish reservoirs and its relationships with the drainage basin area.

Bolshakova, N. & Azuaje, F. (2003) Cluster validation techniques for genome expression data. *Signal Processing,* 83(4)**,** 825-833. 10.1016/S0165-1684(02)00475-9.

Brakstad, F. (1992) A Comprehensive Pollution Survey of Polychlorinated Dibenzo-P-Dioxins and Dibenzofurans by Means of Principal Component Analysis and Partial Least-Squares Regression. *Chemosphere,* 25(11)**,** 1611-1629. Doi 10.1016/0045-6535(92)90309-F.

Brown, C. Discussion of" Sedimentation in reservoirs". *Proc. ASCE.*

Brune, G. M. (1953) Trap Efficiency of Reservoirs. *Transactions American Geophysical Union,* 34**,** 407-418.

Chiomento, J. L. T., Lima, E. P., D'Agostini, M., De Nardi, F. S., Trentin, T. D., Dornelles, A. G., Huzar-Novakowiski, J. & Calvete, E. O. (2021) Horticultural potential of nine strawberry cultivars by greenhouse production in Brazil: A view through multivariate analysis. *Scientia Horticulturae,* 279. ARTN 109738 10.1016/j.scienta.2020.109738.

Cox, A. L., Meyer, D., Botero-Acosta, A., Sagan, V., Demir, I., Muste, M., Boyd, P. & Pathak, C. (under review) Estimating Reservoir Sedimentation Using Deep Learning. *ASCE Journal of Hydrologic Engineering*.

Daly, C., Smith, J. I. & Olson, K. V. (2015) Mapping Atmospheric Moisture Climatologies across the Conterminous United States. *Plos One,* 10(10). ARTN e0141140 10.1371/journal.pone.0141140.

Daszykowski, M., Kaczmarek, K., Heyden, Y. V. & Walczak, B. (2007) Robust statistics in data analysis - A review basic concepts. *Chemometrics and Intelligent Laboratory Systems,* 85(2)**,** 203-219. 10.1016/j.chemolab.2006.06.016.

Davies, D. L. & Bouldin, D. W. (1979) A Cluster Separation Measure. *IEEE Transactions on Pattern Analysis and Machine Intelligence,* PAMI-1(2)**,** 224-227. 10.1109/TPAMI.1979.4766909.

Derbew, S. (2020) Multivariate analysis of hulled barley (Hordeum vulgare L.) landraces of Southern Ethiopia. *Cogent Food & Agriculture,* 6(1). Artn 1841357 10.1080/23311932.2020.1841357.

Dumicic, K., Casni, A. C. & Palic, I. (2015) Multivariate analysis of determinants of Internet banking use in European Union countries. *Central European Journal of Operations Research,* 23(3)**,** 563-578. 10.1007/s10100-014-0371-6.

Emmerson, R. H. C., O'Reilly-Wiese, S. B., Macleod, C. L. & Lester, J. N. (1997) A multivariate assessment of metal distribution in inter-tidal sediments of the Blackwater Estuary, UK. *Marine Pollution Bulletin,* 34(11)**,** 960-968. Doi 10.1016/S0025-326x(97)00067-2.

EPA (n.d.) *Ecoregions*. Available at: https://www.epa.gov/eco-research/ecoregions [Accessed December 2021].

Foster, M. (2020) Developing predictive equations to forecast reservoir sedimentation rates. Bureau of Reclamation.

Garg, V. & Jothiprakash, V. (2008) Trap efficiency estimation of a large reservoir. *ISH Journal of Hydraulic Engineering,* 14(2)**,** 88-101.

Goyal, H., Sandeep, D., Venu, R., Pokuri, R., Kathula, S. & Battula, N. (2014) Normalization of Data in Data Mining. *International Journal of Software and Web Sciences,* 14**,** 32-33.

Graf, W. L., Wohl, E., Sinha, T. & Sabo, J. L. (2010) Sedimentation and sustainability of western American reservoirs. *Water Resources Research,* 46. Artn W12535 10.1029/2009wr008836.

Gu, X. & Angelov, P. Autonomous anomaly detection. *2017 Evolving and Adaptive Intelligent Systems (EAIS)*. 31 May-2 June 2017. 1-8.

Hazarika, B. B., Gupta, D. & Berlin, M. (2020) Modeling suspended sediment load in a river using extreme learning machine and twin support vector regression with wavelet conjunction. *Environmental Earth Sciences,* 79(10). 10.1007/s12665-020-08949-w.

Huang, J. L., Li, Y. F. & Xie, M. (2015) An empirical analysis of data preprocessing for machine learning-based software cost estimation. *Information and Software Technology,* 67**,** 108-127. 10.1016/j.infsof.2015.07.004.

Jiang, Y., Cukic, B. & Menzies, T. Can data transformation help in the detection of fault-prone modules? , *Proceedings of the 2008 workshop on Defects in large software systems*. 16-20.

Jirachan, T. & Piromsopa, K. Applying KSE-test and K-means clustering towards scalable unsupervised intrusion detection. *2015 12th International Joint Conference on Computer Science and Software Engineering (JCSSE)*. 22-24 July 2015. 82-87.

Jolliffe, I. T. & Cadima, J. (2016) Principal component analysis: a review and recent developments. *Philosophical Transactions of the Royal Society a-Mathematical Physical and Engineering Sciences,* 374(2065). ARTN 20150202 10.1098/rsta.2015.0202.

Kocaguneli, E., Menzies, T. & Keung, J. W. (2012) On the Value of Ensemble Effort Estimation. *Ieee Transactions on Software Engineering,* 38(6), 1403-1416. 10.1109/Tse.2011.111.

Lu, H., Moran, C. J. & Sivapalan, M. (2005) A theoretical exploration of catchment-scale sediment delivery. *Water Resources Research,* 41(9). Artn W09415 10.1029/2005wr004018.

Martinez, A. M. & Kak, A. C. (2001) PCA versus LDA. *Ieee Transactions on Pattern Analysis and Machine Intelligence,* 23(2), 228-233. Doi 10.1109/34.908974.

Meharie, M. G. & Shaik, N. (2020) Predicting highway construction costs: comparison of the performance of random forest, neural network and support vector machine models. *Journal of Soft Computing in Civil Engineering,* 4(2), 103-112.

Minear, J. T. & Kondolf, G. M. (2009) Estimating reservoir sedimentation rates at large spatial and temporal scales: A case study of California. *Water Resources Research,* 45. Artn W12502 10.1029/2007wr006703.

Moonesinghe, H. D. K. & Tan, P. Outlier Detection Using Random Walks. *2006 18th IEEE International Conference on Tools with Artificial Intelligence (ICTAI'06)*. 13-15 Nov. 2006. 532-539.

NRCS-USDA (n.d.) Technical Guide to RUSLE use in Michigan. NRCS-USDA State Office of Michigan.

Office of Energy Efficiency & Renewable Energy (n.d.) IECC climate zone map Image.

Patro, S. G. K. & Sahu, K. K. (2015) Normalization: A Preprocessing Stage. *ArXiv,* abs/1503.06462.

Peterson, K. T., Sagan, V., Sidike, P., Cox, A. L. & Martinez, M. (2018) Suspended Sediment Concentration Estimation from Landsat Imagery along the Lower Missouri and Middle Mississippi Rivers Using an Extreme Learning Machine. *Remote Sensing,* 10(10). ARTN 1503 10.3390/rs10101503.

Peterson, K. T., Sagan, V. & Sloan, J. J. (2020) Deep learning-based water quality estimation and anomaly detection using Landsat-8/Sentinel-2 virtual constellation and cloud computing. *Giscience & Remote Sensing,* 57(4), 510-525. 10.1080/15481603.2020.1738061.

Pinson, A., Baker, B., Boyd, P., Grandpre, R., White, K. D. & Jonas, M. (2016) U.S. Army Corps of Engineers Reservoir Sedimentation in the Context of Climate Change. *Civil Works Technical Report, CWTS 2016-05.* Washington DC.: U.S. Army Corps of Engineers.

Reid, M. K. & Spencer, K. L. (2009) Use of principal components analysis (PCA) on estuarine sediment datasets: The effect of data pre-treatment. *Environmental Pollution,* 157(8-9)**,** 2275-2281. 10.1016/j.envpol.2009.03.033.

Richards, K. (1993) Sediment delivery and drainage network. *Channel network hydrology***,** 221-254.

Rousseeuw, P. J. (1987) Silhouettes: a graphical aid to the interpretation and validation of cluster analysis. *Journal of computational and applied mathematics,* 20**,** 53-65.

Sholtes, J. S., Ubing, C., Randle, T. J., Fripp, J., Cenderelli, D. & Baird, D. C. (2018) Managing Infrastructure in the Stream Environment. *Journal of the American Water Resources Association,* 54(6)**,** 1172-1184. 10.1111/1752-1688.12692.

Thomas, C. & Balakrishnan, N. (2009) Improvement in Intrusion Detection With Advances in Sensor Fusion. *Ieee Transactions on Information Forensics and Security,* 4(3)**,** 542-551. 10.1109/Tifs.2009.2026954.

Tillman, F. D. (2015) Documentation of input datasets for the soil-water balance groundwater recharge model of the Upper Colorado River Basin. US Geological Survey.

USACE (n.d.) *National Inventory of Dams*. Available at: https://nid.sec.usace.army.mil/#/ [Accessed January 2022].

USDA (1986) *Urban Hydrology for Small Watersheds*. Available at: https://www.nrc.gov/docs/ML1421/ML14219A437.pdf.

USGS (2016) *National Land Cover Database (NLCD) 2016* Available at: https://www.usgs.gov/centers/eros/science/national-land-cover-database?qt-science_center_objects=0#qt-science_center_objects [Accessed January 2022].

USGS (2017) *1/3rd arc-second Digital Elevation Models (DEMs) - USGS National Map 3DEP Downloadable Data Collection*. [Accessed January 2022].

Viger, R. & Bock, A. (2014) GIS features of the geospatial fabric for national hydrologic modeling. *US Geological Survey*, . https://doi.org/10.5066/F7542KMD.

Walling, D. E. (1983) The sediment delivery problem. *Journal of hydrology*, 65(1-3)**,** 209-237.

Wang, Z. Y. & Hu, C. H. (2009) Strategies for managing reservoir sedimentation. *International Journal of Sediment Research*, 24(4)**,** 369-384. Doi 10.1016/S1001-6279(10)60011-X.

WEST Consultants (2015) Identification and Assessment of Hydrologic Indicators for Predicting Reservoir Sedimentation Rates - Summary Report. *In:* Engineers, U. S. A. C. o. (ed.).

Table 1. Percent of variance (% Var.) held by PC1-PC4 and 10 variables with highest loads (contribution) on PC1-PC4, ranked from left to right. The sign reflects a positive or negative load

PC	% Var	Ranked variables by percentage of contribution to PCs									
1	42.1	DEMMax 9% (+)	BaRlf 8.8% (+)	DEMStd 8% (+)	DEMMean 6.2% (+)	DEMMed 5.9% (+)	BA 5.3% (+)	HydLen 4.8% (+)	Erod 4.5% (-)	MeanPre 4.4% (-)	UpsNorSt 4.1% (+)
2	16.7	OrigCap 6.2% (+)	BA 6.1% (+)	HydLen 6% (+)	SlpMean 5.6% (-)	SedRt 5.5% (+)	UpsNorSt 5.4% (+)	CapLoss 5.2% (+)	UpsDamH 5.1% (+)	UpsMaxSt 5% (+)	CN 4.8% (+)
3	9.6	Forest 16.3% (+)	MeanPre 9.9% (+)	MedPre 8.8% (+)	SlpMean 7.1% (+)	AvLat 6.7% (-)	CumPre 4.6% (+)	BaRlf 4.3% (+)	MaxPre 4.1% (+)	AvLon 3.9% (+)	DEMStd 3.7% (+)
4	7.2	NormPre 9% (+)	AvLat 8.7% (-)	DEMMin 8.2% (-)	MaxPre 8.1% (+)	AvLon 7% (-)	Forest 6.1% (-)	Erod 5.2% (-)	DEMMed 5% (-)	MedPre 4.8% (-)	DEMMean 4.6% (-)

Table 2. Reservoirs with anomalous records flagged by the Autonomous Anomaly Detection (AAD) and the Kolmogorov-Smirnov and Efron (KSE) method with Z-score >2.

Basin ID	IECC Classification	EPA Classification	No. Records Flagged AAD only	No. Records Flagged KSE only	No. Records Flagged AAD & KSE
Basin_2	3	Mediterranean California	0	0	1
Basin_8	3	Mediterranean California	0	3	0
Basin_9	3	Mediterranean California	0	0	2
Basin_12	3	Mediterranean California	0	2	0
Basin_31	4	Great Plains	0	1	0
Basin_32	4	Great Plains	0	1	0
Basin_38	4	Eastern Temperate Forests	1	0	0
Basin_60	4	Eastern Temperate Forests	1	0	0
Basin_64	3	Mediterranean California	0	2	0
Basin_96	4	Eastern Temperate Forests	2	0	0
Basin_100	3	Northwestern Forested Mountains	0	0	1
Basin_108	4	Eastern Temperate Forests	1	0	0
Basin_114	2	North American Deserts	2	0	0
Basin_115	3	Mediterranean California	1	0	0
Basin_126	5	Eastern Temperate Forests	1	0	0
Basin_134	6	Northwestern Forested Mountains	1	0	0
Basin_149	3	Eastern Temperate Forests	1	0	0
Basin_165	5	North American Deserts	1	0	0
Basin_169	5	Northwestern Forested Mountains	0	0	1
Basin_182	5	Northwestern Forested Mountains	0	0	1

FIGURE CAPTION LIST

Figure 1. Data sources and derived variables (numerical and categorical) of the composite RSI dataset.

Figure 2. Location of the 174 reservoirs of the RSI composite dataset.

Figure 3. Plot of variable loads for PC1-PC4. a) PC1 vs. PC2, b) PC3 vs. PC4. See Table S. 1 for variable abbreviations references.

Figure 4. Records classified by EPA ecoregions on a) PC1 vs. PC2 and c) PC3 vs. PC4, respectively; records classified by IECC climate zone on b) PC1 vs PC2 and d) PC3 vs PC4, respectively.

Figure 5. Histogram of the KSE-scores estimated for all records.

Figure 6. Count of potential anomalous records detected by the AAD and KSE methods per reservoir's basin.

Figure 7. K-means clusters plotted in the a) PC1 vs. PC2 and b) PC3 vs. PC4 dimensions. Anomalous records flagged by AAD and KSE methods are specified by marker and labels correspond to Basin ID number.

Figure 8. KSE anomalous records with values outside the mean +/- standard deviation fringe.

Figure 9. AAD anomalous records with values outside the mean +/- standard deviation fringe.